Debris Analysis and Mitigation for Target Motion Systems

Robert Clarke, Phil Rice, Darren Neville, Toby Strange, Alistair Cox, Steve Hook, Christopher Spindloe, Martin Tolley

Central Laser Facility, STFC Rutherford Appleton Laboratory

Harwell Science and Innovation Campus, Didcot, Oxon, OX11 0QX (UK)

Main contact email address: *Rob.clarke@stfc.ac.uk*

Introduction

Laser-target interactions can create a large amount of debris which has the capability to damage optical components within the interaction chambers. Historically, the main protection has been towards the optical components due to the high cost of replacement. The target debris also creates issues for other components within the interaction chambers, which may not be expensive, but are part of the critical operating systems for the facilities. This paper documents the recent investigations into the effect of target debris on the motion systems used in the HPL facilities.

Debris Analysis.

Almost all x,y,z motion systems in use within the experimental chambers on Vulcan and Astra facilities use DC motor systems and Sony Magnescale encoders for position referencing. The only exception to date is the new Gemini inserter system which uses a hexapod design. The standard mounts, commonly referred to as 602's after the original drawing number have been the '*workhorse*' mount style for over 10 years, and the associated technology within the mounts has shown exceptional reliability and functionality. Over the last few years however, the number of problems associated with drive failures has increased. Several factors have contributed to this, ranging from EMP damage in motion controllers to cable faults due to poor cable management. One failure type which has been a re-occurring theme of late is the '*sticking*' of the Sony Magnescale encoders, where the Cu-Ni-Fe alloy, magnetically encoded rod becomes jammed within the read head. Figure 1 shows the standard produce in use, which has a clearance between rod and head of only a few 10's of microns in order to achieve the 0.5µm measurement resolution.

Figure 1. Sony Magnescale rod as used on the existing 602 encoded motion systems.

This '*sticking*' if the rod has been the most common failure mode over the last 2 years, and it is usually fixed by replacement of the magnetic rod in-situ. For complex experiments, this usually means attempting to access the mount whilst negotiating the surrounding diagnostics, and since the 602 design is both compact and low-profile, this replacement usually takes around 30 minutes for an experienced person.

Analysis of rods post-experiment has helped to determine the main cause of this '*sticking*', which was at first believe to be a misalignment of the read head and rod itself. The analysis has revealed instead that the main cause is from target debris coating the rod, and in places depositing large '*blobs*' of target debris. Figure 2 shows one of the images of target debris on one of the rods which caused failure in one of the target mount motions.

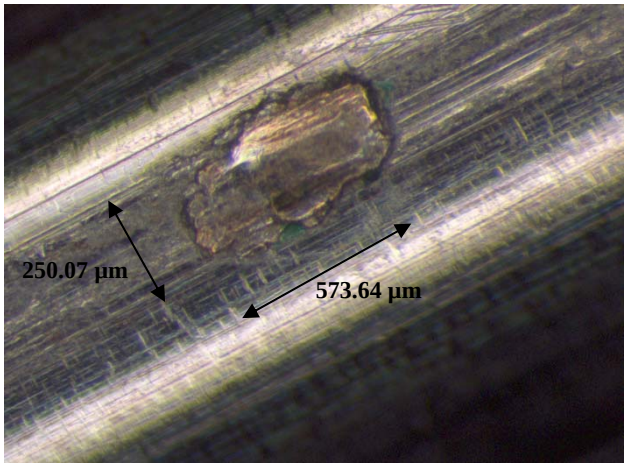

Figure 2. High-resolution optical microscope image of target debris on the Magnescale rod.

The debris observed on the mount is in the order of a few hundred microns in size, and is much larger than the clearance between the rod and read head on the encoder. Tests to determine the contact strength of the debris confirm that it is effectively welded onto the rod surface and is almost impossible to remove without inflicting damage to the encoded rod itself. An Energy Dispersive x-ray Spectroscopy (EDX) image of the section containing the debris allowed the identification of the elements present. This image was taken using the capabilities within the CLF's Target Fabrication Laboratory.

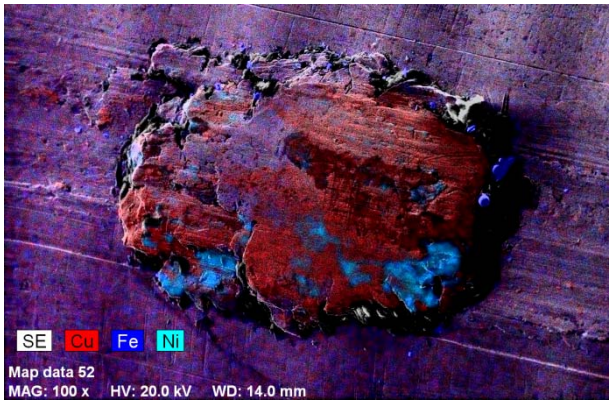

Figure 3. EDX image of target debris coated onto the magnetic rod.

The debris analysis shows a large lump of mainly copper debris welded onto the Magnescale rod. There are also traces of nickel

and other less obvious elements within the debris, all of which can be traced back to target materials used.

Debris Mitigation.

In order to cover the encoders to mitigate against debris, two routes are being investigated. The first is the replacement of all the encoders with enclosed versions of the same technology. This is not ideal, since the enclosed rod versions are much bulkier and would require a major redesign of the mounting system. The associated cost of replacing the encoders on over 20 mounts, each with 3 axis is also fairly significant. The second, preferred route is to add compressible covers onto the rods, which will allow the full freedom of motion without having a significant impact on the design of the mount. Although a final product decision is yet to be made, an example product range is shown in figure 4.

Figure 4. Flexible moulded bellows being investigated for covering the magnetic rod.

Conclusions

The majority of failures of target motion systems over the last few years have been observed to be linked directly to debris production from the laser-target interaction. This finding has enabled the development of the existing 602 3-axis target mounts to be directed towards the mitigation of debris and thus dramatically reducing the expected number of failures in the future. Protection method and hence production type will be directly controlled by the need to maintain a compact mount design as well as minimize the associated cost impact.

Acknowledgements

The authors would like to acknowledge the support of Axis (www.axis-gb.com) who have supplied the CLF with the Sony Magnescale encoders for many years and have been directly involved in the process of identifying the recent failure mechanisms.

Calibration of Image Plate response to energetic Carbon ions

Contact *d.doria@qub.ac.uk*

D. Doria, S. Kar, K. Kakolee , B. Ramakrishna, G. Sarri, K. Quinn, M. Borghesi
Centre for Plasma Physics, Queen's University Belfast, Belfast, BT7 1NN

J. Osterholz, M. Cerchez, O. Willi
Institute of Laser and Plasmaphysics, Heinrich-Heine-University Düsseldorf, Germany

X. Yuan, P. McKenna
SUPA, Department of Physics, University of Strathclyde, Glasgow G4 0NG, UK

Introduction

A wide range of detectors has been developed to reveal the different existing types of radiation. Among those there are solid state detectors such as CR39, which is used as a nuclear track detector for particle counting; films with an active medium consisting of an emulsion (e.g.. radiochromic films (RCF)); photodiodes; CCDs; photomultipliers (PMT); electron multipliers (EMT); microchannel plates (MCP); probes such as Faraday cups; scintillators (glasses, plastics, gases, liquids, crystals). Scintillators use the principle of photoluminescence (PL) that occurs when an atom is excited to a higher energy state and then returns to a lower one at a later time. PL is characterized by two forms of luminescence: fluorescence and phosphorescence. Typically a scintillator is made of fluorescent material and releases the energy in a short time (less than microseconds). The image plate (IP) is made of phosphors with phosphorescent properties which can release the stored energy in a long-lasting de-excitation (few hours). The IP is fabricated depositing $BaFX:Eu^{2+}$ (X=Cl,Br) crystal grains on a polyester support film. The grains have a size of about 5µm and are kept together by means of a urethane resin [1]. The energy stored in the IP can be retrieved by stimulating the excited metastable state. The stimulation can be done by photons, and then the energy is released as light and called photo-stimulated luminescence (PSL). The IP is read using a scanner. The surface of the IP is scanned by a laser diode that de-excites the metastable state generating UV light which is read by a photo-multiplier tube (PMT) and then converted in an electric signal. The output signal of the PMT is proportional to the light illuminating it. The signal is digitized by an analog-to-digital converter (ADC) and an algorithm in a 16bit discrete number. This quantization allows to store the signal as a 16bit TIFF image, in which each pixel represents a scanned position on the IP surface. The spatial resolution is typically 25µm or 50µm, but some scanners can go up to 5µm resolution. The IP has a high sensitivity to the stimulating radiation and the response is linear [2]. The IP dynamic range is very high, but the scanner settings can give a reading of five orders of magnitude at best. In any case, the IP can be scanned more than once if necessary. Once used, the IP can be erased by exposing it to intense light for at least 15min.
The response of the Image Plate detector to protons has been reported in earlier works [3,4]. We discuss here some measurements in which the IP response to Carbon ions has been measured by cross-calibration with CR39.

Experimental set-up and methods

The measurements were carried out in the Target Area Petawatt (TAP) . The VULCAN laser operates in the infrared range at a wavelength of 1053 nm. The laser pulse is compressed using the Chirped pulse amplification (CPA) technique obtaining pulse duration of sub-picosecond (~700 fs). The laser beam was focused onto a thin metal foil, typically Cu or Au by using an f/3 off-axis parabolic mirror and a plasma mirror. The laser pulse energy typically used is about 450 J in a ~ 10-20 µm focal spot. The laser energy losses due to compressor gratings and plasma mirror were measured using a calorimeter, and they are 50% and 20%, respectively; giving a total energy loss of 40%. and a laser intensity on target up to $3 \cdot 10^{20}$ W/cm^2. Such an intense laser pulse can generate proton and ion beams by means of the Target Normal Sheath Acceleration (TNSA) mechanism [5]. These ions originate from hydrocarbons and water vapour impurities usually present on the target surface. Owing to this acceleration mechanism broadband particle sources are generated with energy cut-off up to tens of MeV/nucleon [6]. A Thomson Parabola (TP) was used as mass spectrometer to discern the different ion species present in the ion source.
The TP was mounted in axis with the laser and placed at the rear side of the target. The distance between target and TP pinhole was 630 mm. IP and CR39 were used as detectors (see Fig. 1). In order to calibrate the dispersion power of the spectrometer, the IPs were filtered to obtain a known energy cut-off of proton by performing a few laser shots.
A comparison of the cut-off positions along the dispersion plane with the analytical calculations gives a relationship between ion energy and position on the detector.

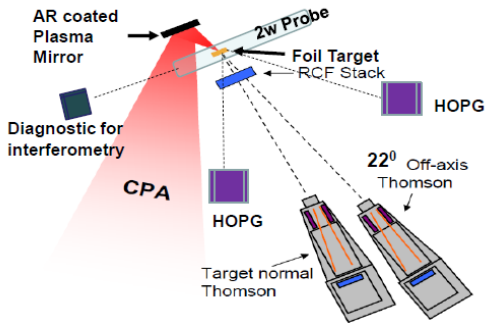

Figure 1. Layout of the experimental set up

IP characteristics

IP from Fuji Photo Film Co. Ltd is composed of a photostimulable phosphor layer made of very small crystals with a grain size of about 5µm and a density of 5.2 g/cm^3. Among several types of IP the BAS-TR2025 has been chosen in this experiment. For this type of IP the phosphor layer thickness and density are 50µm and 2.85 g/cm^3, respectively [7]. Its main feature is the absence of the plastic protective layer usually present in the most of the other types of IPs. The purpose of the layer is to preserve the response efficiency of the phosphor active medium by avoiding its degradation. However, it also slows down the fast ions and can even stop low energy ions before they reach the active phosphor layer, then making them undetectable. The typical thickness of the protective layer is about 10 µm. This thickness is sufficient to stop protons and carbon ions with energy per nucleon below about 800 keV/amu.
The IP can store the energy received by the impacting particles owing to the excitation of a metastable state of the phosphor, but on the other hand and for the same reason it has an intrinsic fading out time. Experimentally, it has been shown that the

phosphor releases the energy with two different decay times [2,3].
The metastable state de-excites first with a fast decay time losing about 20% of the stored signal in 20min and then with a longer decay time bringing the initial signal to 60% of its value in about 3hr.

CR39 characteristics
The CR39 is a plastic polymer used as solid state detector in nuclear science to detect ion, proton and neutron; it is insensitive to other forms of radiation. These particles leave trails when they travel through the bulk material and deposit their energy slowing down according to the stopping power theory. A typical CR39 plate has a thickness of about 1 mm and density of 1.3 g/cm^3. 1mm thick CR39 is able to stop (and detect) proton and Carbon ion with energy up to 10 MeV and 230 MeV, respectively. The tracks left in the bulk are revealed by etching the CR39 in a sodium hydroxide solution. As the etching time increases the tracks get larger, creating pits on the surface. The etching was made in a 6.0N NaOH solution at a temperature of about 70°C for 15 minutes. Throughout the etching and counting procedure attention was paid to get pits clearly visible and avoid overlapping.

Result
In order to obtain the calibration of the IP BAS-TR2025 for Carbon ions of different energies a TP is used to disperse the ion beam onto the CR39 and IP. A slotted CR39 placed on the IP was used as detector so that carbon ions having reasonably close energy can be recorded at the same time around the edges of the slots, both on the CR39 and IP. After etching, the CR39 was observed with an optical microscope. Images of the pits distributed along the dispersion axis were grabbed using a CCD and then the pits around the edges of the slots were easily counted. Below, in Figure 2, an image representative of the pits' trace in the region of the slot edge is shown.

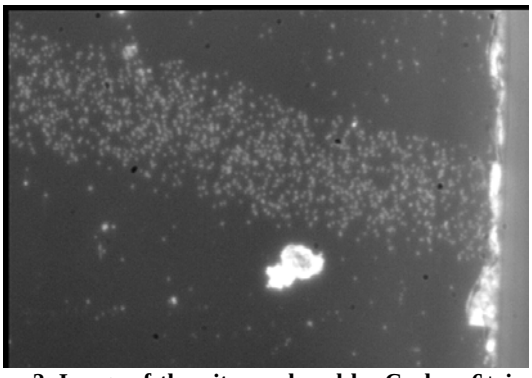

Figure 2. Image of the pits produced by Carbon 6+ ions in the region of a slot edge of theCR39 (right-hand side). The image is taken with a magnification 10x. The analysis is done using greater magnification.

The IP was read using the Fuji Film FLA-5000 scanner with a scanning pixel resolution of 50µmx50µm, sensitivity of 5000 and latitude of 5. The output is a TIFF image that holds information about the PSL strength in a 16bit integer number. Using the algorithm provided with the scanner specifications it is possible to get back the PSL strength per pixel, which is proportional to the energy released by the particles hitting a particular pixel area. The relationship between particle energy and position on the detector is obtained by using a code in which the motion of a particle passing through the TP is calculated. Figure 3 shows the IP scan image used for the calibration. A Cu target 500 nm thick was used in this shot.

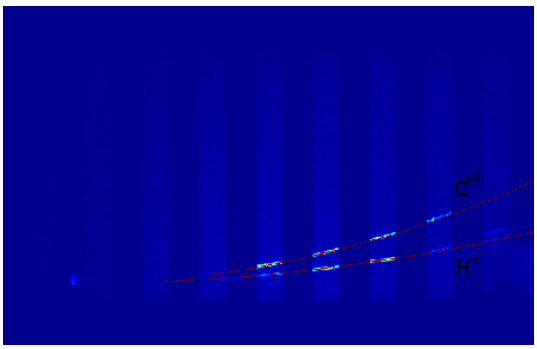

Figure 3. IP scan image showing the shadow of the CR39 slots and proton and carbon +6 ion signals. The red curves are the theoretical fits obtained using the above-mentioned code.

Owing to the code, dN/dE(E), i.e the number of pits per unit energy and PSL/dE(E), i.e. the equivalent PSL strength per unit energy, are obtained as a function of the carbon energy E. Each experimental point represents an edge of the CR39. In this way, it was possible to obatined 9 data points for fully ionized carbon ions. The calibration curve is the ratio of PSL/dE(E) to dN/dE(E) that gives the PSL value per carbon atom as a function of the carbon energy, CAL=PSL/#C(E). The function CAL(E) was multiplied by a correction factor to take into account the fade out time due to the spontaneous de-excitation of the IP phosphor. The correction factor is obtained from Ref.2, for the same type of IP.
Figure 4 shows the calibration curve for carbon ion with energy up to 40 MeV. The peak of the sensitivity curve appears to be around 27 MeV.

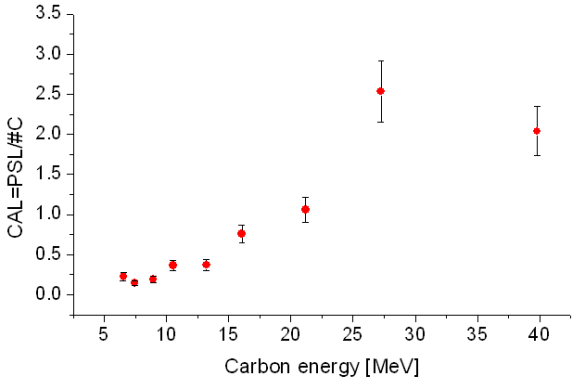

Figure 4. Calibration curve that relates the PSL signal to the number of carbon ions as function of the ion energy.

Conclusion
The absolute sensitivity of the IP BAS-TR2025 has been calculated by comparing the PSL value read by the scanner Fuji Film FLA-5000 to the number of carbon ions estimated by using the CR39. The readout value can be slightly different depending on the readout system [3,4].

Acknowledgments
This work was granted by EPSRC (LIBRA Consortium, Grant No: EP/E035728/1) and by STFC Facility access. We acknowledge the support of all staff at CLF, RAL.

References
1.http://www.fujifilm.com/products/life_science/index_en.html
2. I J Paterson *et al*., *Meas. Sci. Technol*. **19,** 095301 (2008).
3. A Mančić *et al*., *Rev. Sci. Instrum.* **79,** 073301 (2008).
4. I WChoi *et al*., *Meas. Sci. Technol*. **20,** 115112 (2009).
5. Snavely R A *et al., Phys. Rev.Let,*. **85,** 2945–8 (2000).
6. J. Fuchs *et al., Nat. Phys.* **2,** 48 (2006).
7. B. Hidding *et al., Rev. Sci. Instrum.* **78**, 083301 (2007).